

1746

192
3-26-81
JWH

R-3064

(1)

D. 2437

FEBRUARY 1981

PPPL-1746

UC-20f

MASTER

NON-RESONANT PARAMETRIC DECAY
OF LOWER-HYBRID WAVES IN THE
ACT-1 TOROIDAL DEVICE

BY

K. L. WONG AND M. ONO

**PLASMA PHYSICS
LABORATORY**



DISTRIBUTION OF THIS DOCUMENT IS UNLIMITED

**PRINCETON UNIVERSITY
PRINCETON, NEW JERSEY**

This work was supported by the U.S. Department of Energy
Contract No. DE-AC02-76-CMO 3073. Reproduction, translation,
publication, use and disposal, in whole or in part,
by or for the United States government is permitted.

Non-Resonant Parametric Decay of Lower-Hybrid
Waves in the ACT-1 Toroidal Device

King-Lap Wong and Masayuki Ono

Plasma Physics Laboratory, Princeton University
Princeton, New Jersey 08544

ABSTRACT

Non-resonant parametric decay of lower-hybrid waves, observed in a number of high-power tokamak rf heating experiments, is positively identified as a decay into ion-cyclotron quasi-modes. The decay-wave spectrum, wavelength and amplitude profile are measured inside a toroidal plasma with pump frequency $f_0 \sim 3.5 f_{pi} \sim 25 f_{ci}$.

DISCLAIMER

This document contains information which is classified as "Confidential" under Executive Order 12958, Section 1.4. The information is being disseminated to you in confidence. It is not to be distributed outside your organization without the express approval of the originating agency. If you are not an authorized recipient, you should not disseminate this information. If you are an authorized recipient, you should not disseminate this information outside your organization without the express approval of the originating agency. The use and release of this information is subject to the security, privacy and other policies of the United States Government and its agencies.

11A

Lower-hybrid wave heating of magnetized plasmas is a promising candidate for tokamak ignition because of the readily available microwave power and the desirable features of slow-wave coupling structure/phased-waveguide arrays. However, at the high power levels required for tokamak heating, various nonlinear phenomena can occur. One well-known nonlinear phenomenon is the parametric decay¹⁻⁷ of lower-hybrid waves in which the frequencies of the decay waves are observed to be separated roughly by the ion cyclotron frequency, f_{ci} . This decay spectrum has become a characteristic of lower-hybrid wave heating in tokamaks. It has been observed in ATC,⁶ JFT-2,⁷ Doublet-IIA,⁸ WEGA,⁹ PETULA,¹⁰ and Alcator A.¹¹ In all these experiments, the decay frequency spectrum was detected by a probe placed in the limiter shadow but, because of the difficulties in wavelength measurements, the component waves were never identified. Various conjectures were made, based on the observed decay spectrum. The spectrum has been attributed to non-resonant decay (lower-hybrid wave + lower-hybrid wave + ion cyclotron quasi-mode) in the ATC experiment,⁶ and to resonant decay (lower-hybrid wave + lower-hybrid waves + ion cyclotron waves) in the JFT-2 experiment.⁷ In this paper, we present the first positive experimental confirmation for the former interpretation, namely, the non-resonant decay of lower-hybrid waves in a toroidal plasma. Unlike previous linear machine experiments,^{12,13} the wave in the present experiment was excited by a slow wave structure in the frequency range $f_0 \sim 3.5 f_{pi} \sim 25 f_{ci}$, very similar to the tokamak experiments. Moreover, the result indicates that toroidal geometry may have an important effect on the decay threshold. Therefore the experiment described here provides a good simulation of the parametric decay process that can occur near the tokamak edge, which process can be critically important^{4,5} to the heating efficiency. However, the final determination of the amount of pump depletion

that may occur in a high-power tokamak heating experiment still awaits further theory and experimentation.

The following parametric dispersion relation¹ has been derived from dipole pump approximation:

$$\begin{aligned}
 1 + \frac{1}{\chi_i} = & J_0^2(\mu) \frac{\chi_e}{1 + \chi_e} + J_1^2(\mu) \left(\frac{\chi_e^+}{1 + \chi_e^+} + \frac{\chi_e^-}{1 + \chi_e^-} \right) \\
 & + \frac{J_0^2(\mu) J_1^2(\mu) \left[\chi_e / (1 + \chi_e) - \chi_e^+ / (1 + \chi_e^+) \right]^2}{1 + 1/\chi_i^+ - J_0^2(\mu) \chi_e^+ / (1 + \chi_e^+) - J_1^2(\mu) \chi_e / (1 + \chi_e)} \\
 & + \frac{J_0^2(\mu) J_1^2(\mu) \left[\chi_e / (1 + \chi_e) - \chi_e^- / (1 + \chi_e^-) \right]^2}{1 + 1/\chi_i^- - J_0^2(\mu) \chi_e^- / (1 + \chi_e^-) - J_1^2(\mu) \chi_e / (1 + \chi_e)} \quad (1)
 \end{aligned}$$

where μ is the parametric coupling coefficient¹; χ_i and χ_e are the ion and electron susceptibilities for the low frequency decay waves and the superscripts "+" and "-" refer to the upper and lower sideband modes; J_0 and J_1 are the Bessel functions of the first kind. Equation (1) has been solved numerically¹ for the growth rate of the decay instability. The calculation can be greatly simplified with the following assumptions which are well justified in our experiment: (a) $\mu^2 \ll 1$, (b) $|\chi_i| \gg |\chi_i^+|$, $|\chi_e| \gg |\chi_e^+|$, (c) $1 + \chi_i^- + \chi_e^- = 0$, $1 + \chi_i^+ + \chi_e^+ \neq 0$. Then the growth rate can be calculated from¹

$$\gamma = -\Gamma_2 - \frac{\mu^2}{4|\partial/\partial\omega_2 [\text{Re}(1 + \chi_i^- + \chi_e^-)]|} \text{Re} \frac{1/\chi_i}{1 + \chi_i + \chi_e} \quad (2)$$

where "Re" denotes the real part of a complex quantity; ω_2 and Γ_2 are the frequency and the damping rate of the sideband mode. Figure 1 shows the calculated growth rate as a function of the decay wave frequency for our experimental parameters. Collisional damping and electron Landau damping are included in Γ_2 , and the parallel wave number (k_{\parallel}) of the decay wave is used as a free parameter to maximize the growth rate. The periodic variation of the growth rate (with period $\sim f_{c1}$) is due to oscillations in the ion susceptibility as a function of frequency. This behavior will explain the decay spectrum shown in Figure 2b. The convective decay threshold can be estimated from¹

$$\gamma > \pi v_2 / L_z, \quad (3)$$

where L_z is the antenna length and v_2 is the parallel phase velocity of the sideband. Equation (3) assumes that the decay waves grow by a factor of e^{π} in one transit through the pump region. However, in a toroidal plasma, the decay waves can go through the toroidal pump region more than once and the decay threshold can be lower than that predicted by Eq. (3). This interesting phenomenon is, we believe, the explanation for the low threshold observed in our experiment.

The experiment was performed in the Princeton ACT-1 device which is a steady-state toroidal machine operating at the following parameters: toroidal field $B_0 \leq 5.6$ kG, plasma density $n \sim 1 - 6 \times 10^{10} \text{ cm}^{-3}$, electron temperature $T_e \sim 5$ eV, ion temperature $T_i \sim 1.5$ eV (determined by test waves near the ion cyclotron frequency),¹⁴ neutral hydrogen pressure 5×10^{-5} Torr (gauge). The plasma has a minor radius $a \approx 9$ cm, and major radius $R = 59$ cm. Lower-hybrid waves at 160 MHz are excited by an 8-ring antenna¹⁵ with parallel wavelength

$\lambda_{\parallel} \approx 6$ cm. Figure 2a shows, in schematic fashion, the experimental setup, and a typical parametric-decay spectrum is shown in Fig. 2b. Upon varying the magnetic field, the frequency of the low-frequency oscillations may be seen to increase with the ion cyclotron frequency, as in Fig. 2c. The calculated frequency is slightly higher than the experimental value. This differential appears because the rf power is fed from the low field side and the pump amplitude peaks at a magnetic field lower than the field on the minor axis.

Figure 3 depicts the experimental setup for perpendicular interferometric wavelength measurements. The parallel wavelength is measured by the phase shift between two probes 5 mm apart situated on the same field line. The first sideband ($\lambda_{\perp} \sim 2.5$ mm, $\lambda_{\parallel} \sim 3.7$ cm) is identified as a lower-hybrid wave that obeys the dispersion relation $\omega \approx \omega_{pe} k_{\parallel} / k_{\perp}$. Waves in the other sidebands are not sufficiently coherent for clean interferograms, indicating that they propagate with a wide range of k_{\perp} which washes out the interference fringes. The measured wave number and frequency show that $1 + \chi_i + \chi_e \neq 0$ for the low-frequency decay wave which must therefore be a forced oscillation (quasi-mode) that can exist only in the presence of the pump field. This behavior is true as well in tokamaks and can be understood as follows: a weakly damped electrostatic wave must have $\omega/k_{\parallel} \gtrsim 3 V_{Te}$ or $\omega/k_{\parallel} \lesssim 0.1 V_{Te}$ in order to avoid strong electron Landau damping; such a condition cannot be satisfied with $\omega \sim n\omega_{ci}$ ($n = 1 - 10$) in typical tokamak lower-hybrid wave experiments where $\omega_0 \sim 25 \omega_{ci}$, $\omega_0 \lesssim 5 \omega_{pi}$. Therefore, resonant decay into electrostatic waves is prohibited under these conditions.

Figure 4 shows radial profiles for the pump and decay-wave amplitudes. The pump wave is localized along the resonance cone trajectory near the antenna (30 cm from center of antenna) where the measurement was made. The first sideband spreads outside the pump; the second sideband (and also the 3rd

and 4th sidebands) propagates all over the plasma, again indicating a wide spread in k_{\perp} . Unlike the sidebands, the low-frequency decay waves are not normal modes of the plasma. They are heavily damped outside the pump region and therefore their amplitudes drop abruptly outside the pump resonance cone. From these data, it is obvious that the decay-wave spectrum has a strong spatial dependence. In tokamak experiments, probes can only survive inside the limiter shadow. Conclusions concerning the variation of the parametric decay instability at various plasma parameters⁷ based on signals from a fixed probe should be treated with caution.

At the operating density $n \approx 5 \times 10^{10} \text{ cm}^{-3}$, the decay threshold is about 25 watts net forward power which corresponds to $E_0 \lesssim 140 \text{ V/cm}$. It is lower than the convective threshold ($E_0 \sim 200 \text{ V/cm}$) calculated from Eq. (3) but much higher than the uniform pump threshold ($E_0 \sim 30 \text{ V/cm}$). At low densities ($n \sim 10^{10} \text{ cm}^{-3}$), the decay threshold becomes closer to the uniform pump threshold because the pump wave can cross the plasma center ($r = 0$) and spreads out.

In conclusion, in an experiment on the ACT-1 toroidal plasma, we have identified the parametric decay of the lower-hybrid wave into an ion-cyclotron quasi-mode. The results, which are in good agreement with theory, are highly pertinent to high-power lower-hybrid heating experiments on tokamaks where the occurrence of such parametric decay at the plasma edge may seriously reduce the rf heating efficiency.

ACKNOWLEDGMENTS

One of the authors (K.L.W.) would like to thank Professors M. Porkolab, A. Bers, and T. H. Stix for helpful discussions. Technical assistance by Messrs. J. Taylor, W. Kineyko, and G. Wurden is gratefully appreciated.

This work supported by the U. S. Department of Energy Contract No. DE-AC02-76-CHO-3073.

REFERENCES

- ¹M. Porkolab, Phys. Fluids 17, 1432 (1974); also Phys. Fluids 20, 2058 (1977).
- ²K. L. Wong, P. Bellan, and M. Porkolab, Phys. Rev. Lett. 40, 554 (1978); also K. L. Wong, J. R. Wilson, and M. Porkolab, Phys. Fluids 23, 96 (1980).
- ³V. K. Tripathi, C. Grebogi, and C. S. Liu, Phys. Fluids 20, 1525 (1977).
- ⁴L. Chen and R. L. Berger, Nucl. Fusion 17, 779 (1977).
- ⁵E. Villalon and A. Bers, Nucl. Fusion 20, 243 (1980).
- ⁶M. Porkolab, S. Bernabei, W. M. Hooke, R. W. Motley, and T. Nagashima, Phys. Rev. Lett. 38, 230 (1977).
- ⁷T. Imai, T. Nagashima, T. Yamamoto, K. Uehara, S. Konoshima, H. Takeuchi, H. Yoshida, and N. Fujisawa, Phys. Rev. Lett. 43, 586 (1979).
- ⁸J. Lohr, V. S. Chan, A. F. Lietzke, J. L. Luxon, C. P. Moeller, and D. F. Vaslow, Bull. Am. Phys. Soc. 22, 1163 (1977).
- ⁹C. Gormezano, P. Blanc, M. Durvaux, W. Hess, G. Ichtchenko, P. Lallia, R. Magne, T. K. Nguyen, H. D. Pacher, G. W. Pacher, F. Soldner, G. Tonon, and J. G. Wegrowe, Proceedings of the 3rd Topical Conference on Radio Frequency Plasma Heating, California Institute of Technology (1978), paper A3.
- ¹⁰P. Briand, L. Dupas, S. N. Golovato, C. M. Singh, G. Melin, P. Grelot, R. Legardeur, and S. Zymanski, Proceedings of the Seventh International Conference on Plasma Physics and Controlled Nuclear Fusion Research held by IAEA at Innsbruck, 23-30 August 1978, Vol. I, p. 65 (IAEA, Vienna, 1979).
- ¹¹J. Schuss, Private Communication.
- ¹²G. R. Allen, D. K. Owens, S. W. Seiler, M. Yamada, H. Ikezi, and M. Porkolab, Phys. Rev. Lett. 41, 1045 (1978).
- ¹³M. Ono, M. Porkolab, and R. P. H. Chang, Phys. Fluids 23, 1675 (1980).

¹⁴M. Ono and K. L. Wong, Phys. Rev. Lett. 45, 1105 (1980).

¹⁵K. L. Wong, R. Horton, and M. Ono, Phys. Rev. Lett. 45 117 (1980).

FIGURE CAPTIONS

- Figure 1. Variation of growth rate as a function of decay wave frequency at $n = 5 \times 10^{10} \text{ cm}^{-3}$, $B_0 = 3.8 \text{ kG}$, $T_e = 5 \text{ eV}$, $T_i = 1.5 \text{ eV}$ (hydrogen plasma).
- Figure 2. (a) Schematic of the ACT-1 device.
 (b) Parametric decay spectrum at $n \sim 5 \times 10^{10} \text{ cm}^{-3}$, $B_0 \approx 3.8 \text{ kG}$, $T_e \sim 5 \text{ eV}$, $T_i \sim 1.5 \text{ eV}$ (hydrogen).
 (c) Variation of decay wave (low frequency daughter wave) frequency with magnetic field at plasma center ($r = 0$). The solid line shows the decay wave frequency for which Eq. (2) give the maximum growth rate.
- Figure 3. Schematic of the experimental setup for interferometry measurements.
- Figure 4. Radial amplitude profiles of the pump, sideband and low frequency decay waves at $B_0 \sim 3.8 \text{ kG}$, $n \sim 4 \times 10^{10} \text{ cm}^{-3}$. (a) Pump, (b) first sideband, (c) first low frequency decay wave, (d) pump, (e) second sideband (f) 2nd low frequency decay wave.

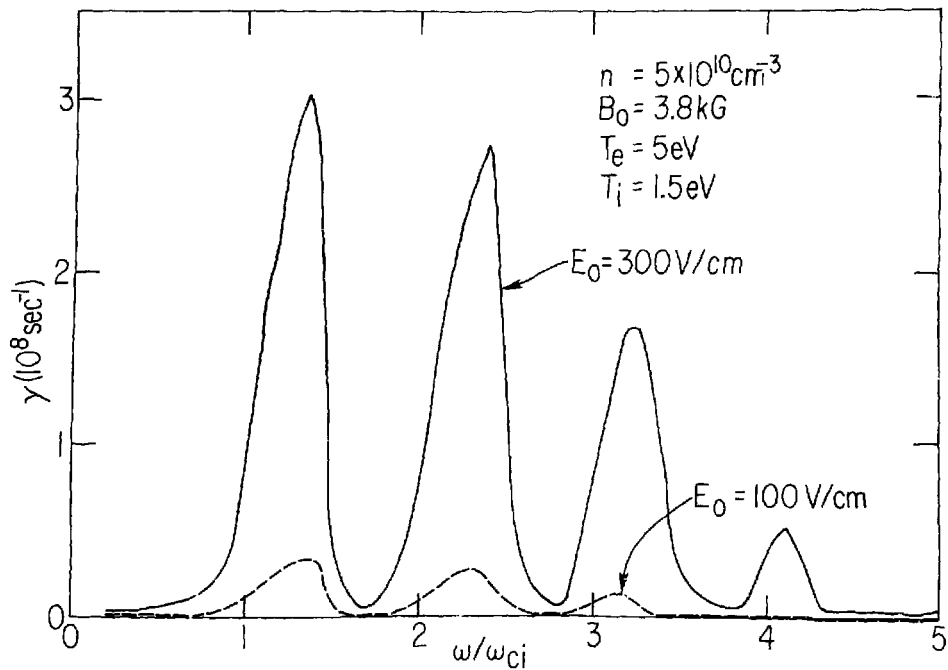


Fig. 1. (PPPL-809101)

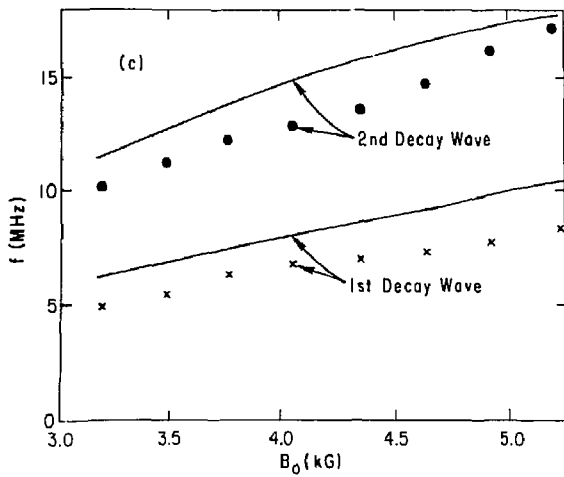
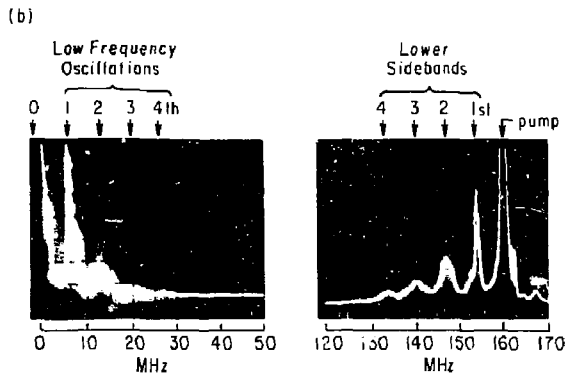
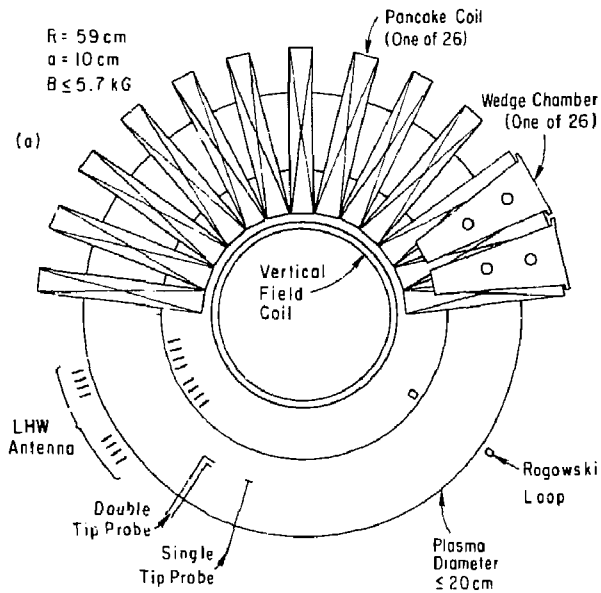


Fig. 2. (PPPL-809147)

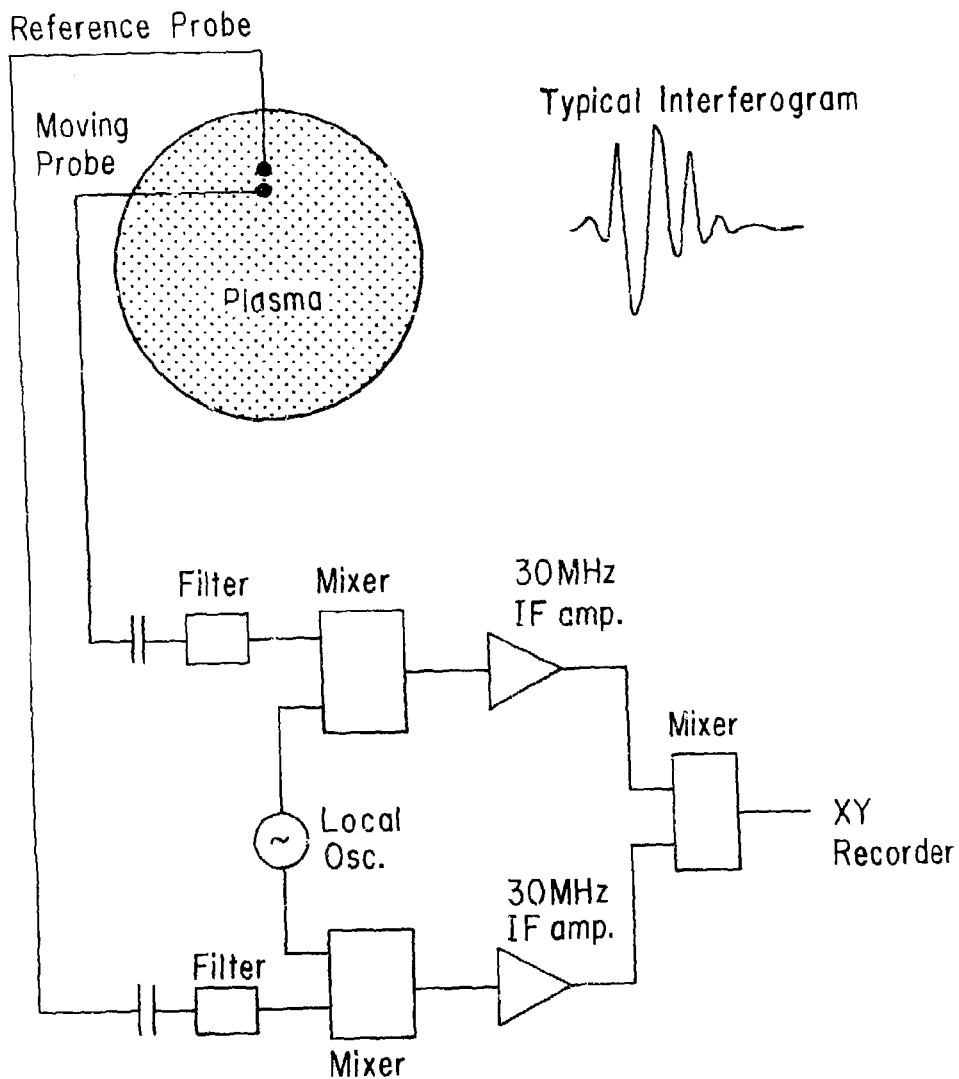


Fig. 3. (PPPL-806999)

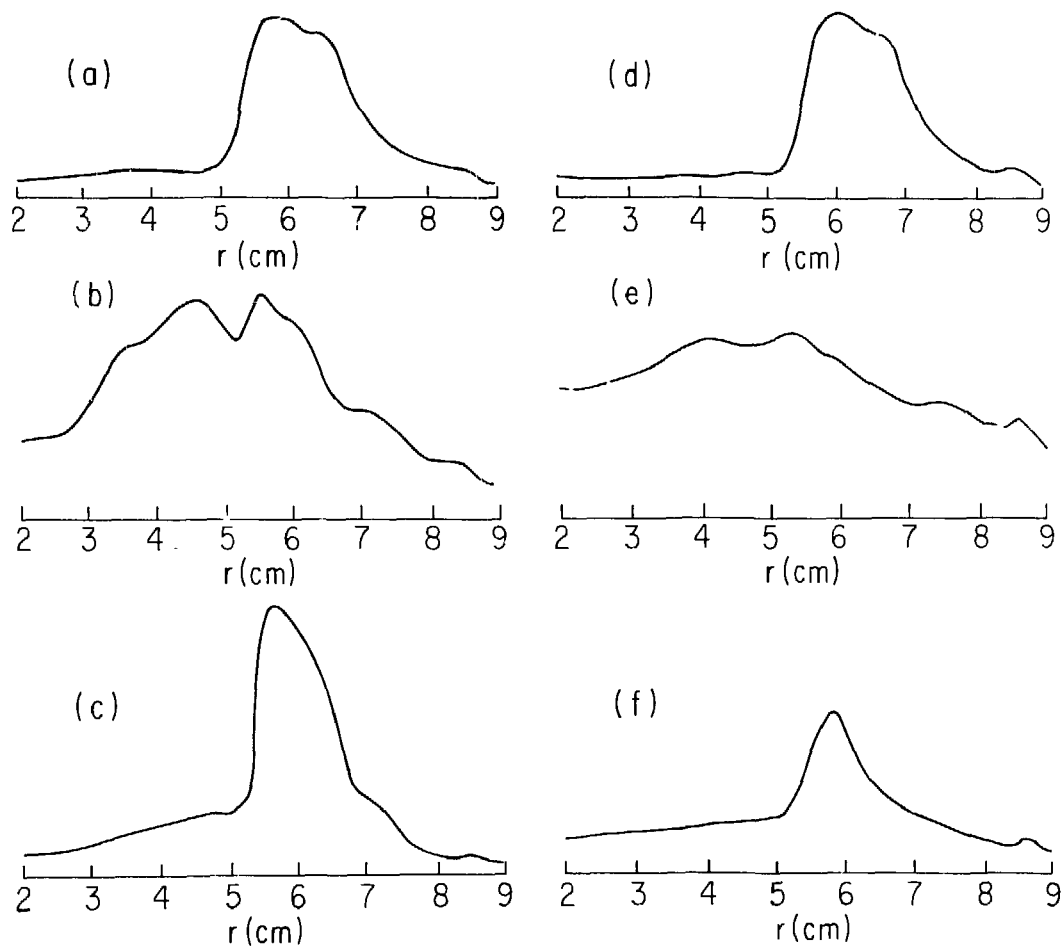


Fig. 4. (PPPL-806998)